Composites

Transition from microcellular to nanocellular chain extended poly(lactic acid)/hydroxyl-functionalized graphene foams by supercritical CO_2

Xianzeng Wang[1,2], Jianguo Mi[3], Hongfu Zhou[1,2,*] , and Xiangdong Wang[1,2,*]

[1] School of Materials and Mechanical Engineering, Beijing Technology and Business University, Beijing 100048, People's Republic of China

[2] Beijing Key Laboratory of Quality Evaluation Technology for Hygiene and Safety of Plastics, Beijing 100048, People's Republic of China

[3] State Key Laboratory of Organic-Inorganic Composites, Beijing University of Chemical Technology, Beijing 100029, People's Republic of China

ABSTRACT

Currently, preparing nanocellular semi-crystalline polymer foams by supercritical CO_2 is a big and newly developing challenge. In this paper, chain extender (CE) and hydroxyl-functionalized graphene (HG) were introduced into poly(lactic acid) (PLA) through melt blending method to improve the crystallization behaviors, rheological properties and foaming behaviors of PLA. Differential scanning calorimetry results showed that the cold crystallization temperature of chain extended PLA (CPLA)/HG was higher 8.2 °C than that of CPLA, due to the introduction of HG and the strong interaction between CPLA and HG. The viscoelasticity of PLA was improved by the addition of CE and HG, due to the formation of branching structure and the interaction between CPLA and HG. Compared with that in PLA/HG, HG aggregation in CPLA/HG became many but small, indicating that the aggregation of HG in the matrix released. A facile batch foaming method with constant foaming temperature slightly lower than melting temperature was employed to fabricate nanocellular PLA foams in the presence of supercritical CO_2. The transition temperature from microcells to nanocells in various PLA foams was confirmed. The effect of chain extension, foaming temperature and the introduction of HG on cell size, cell density, cell size distribution and volume expansion ratio (VER) was studied systematically. For the CPLA/HG foam prepared at 130 °C, its cell size could reach 350 ± 247 nm as well as its cell density and VER were 1.76×10^{13} cells/cm^3 and 3.71 ± 0.16 times, respectively. Finally, the foaming mechanism for the nanocell formation was proposed and explained by schematic diagram.

Address correspondence to E-mail: zhouhongfu@th.btbu.edu.cn; wangxid@th.btbu.edu.cn

Springer

Introduction

Nanocellular polymer foams as a kind of novel and advanced material have the average cell size less than 1 μm and the cell density greater than 10^{12} cells/cm^3, which have attracted wide attention in academic and industrial fields in recent years [1–3]. Nanocellular polymer foams possess high toughness, low thermal conductivity and excellent electrical properties [4], which could be used widely in the fields of insulation materials, separation membranes, sensors and filters [5–7].

In general, the preparation methods of nanocellular polymer foams mainly include: phase separation method [8], batch foaming method [1], extrusion foaming method [3], etching method [9], leaching method [10], thermal decomposition method [11] and so on. Among these, the phase separation method and leaching method need to use a large number of solvents, which were time-consuming, labor-intensive, not economical and environmentally friendly. Etching method and thermal decomposition method generally require sacrificing part of the molecular structure of polymer matrix, for example chain scission, causing damage to the properties of the polymer itself. Compared with other foaming methods, the batch foaming method is the most used method for preparing nanocellular polymer foams and has some advantages, such as low cost, high efficiency, no damage to the environment and the molecular structure of the polymer matrix [12].

Nanocellular poly(methyl methacrylate-co-ethyl acrylate) (PMMA-co-EA) and poly(methyl methacrylate-co-ethyl methacrylate) foams were produced by a solid batch foaming process with supercritical CO_2, in the presence of silica nanoparticles or polyhedral oligomeric silsesquioxane. The results showed that after a post foaming treatment in water bath at 70 °C for 3 min, a medium-density nanocellular PMMA-co-EA foam with 0.5 wt% silica nanoparticles was produced with the cell size of 95 nm, the cell density of 8.6×10^{15} cells/cm^3, and the volume expansion ratio (VER) of 4.88 [13]. A low-temperature pathway to create polycarbonate (PC) nanofoams was reported by Guo and Kumar, which was based on saturating PC in liquid CO_2 at − 30 °C for 72 h. The resultant homogenous PC nanofoams possessed the cell size in the range of 20–30 nm, the cell nucleation density over 10^{15} cells/cm^3 [14]. Throughout the analysis of previous studies, it could be found that the investigations on the nanocellular polymer foams were concentrated on the amorphous polymer using solid batch foaming method. Currently, the preparation of nanocellular semi-crystalline polymer using the melt batch foaming method was still very difficult, because the crystalline region formed during the depressurization and cooling period would influence the cell nucleation and cell growth of semi-crystalline polymer as well as impede the solubility and diffusibility of blowing agent. Recently, nanocellular semi-crystalline poly(lactic acid) (PLA) foams were fabricated by controlling the viscosity, branching and crystallization of PLA in the presence of supercritical N_2 [15].

Supercritical CO_2 as an environment-friendly physical foaming agent for polymer, has some merits such as non-toxic, non-flammability, low global warming potential and ozone depletion potential, and safe in performance [16, 17]. Compared with supercritical N_2, the diffusivity of supercritical CO_2 was higher, leading to the rapid cell nucleation and cell growth, the easily cell mergence and the large cell size [18]. Therefore, the preparation of nanocellular semi-crystalline polymer foams using supercritical CO_2 is a big and newly developing challenge worldwide.

In our research, PLA as one of the typical biodegradable polymer was chosen to produce nanofoams, which was modified with chain extender (CE) and hydroxyl-functionalized graphene (HG) to improve its crystallization and melting behaviors, viscoelasticity, and foaming properties. A batch foaming approach was employed to prepare nanocellular PLA foams, in which the foaming temperature was constant and slightly lower than melting temperature (T_m) for 2 h. The effect of introduction of HG, foaming temperature and the chain extension on the crystallization and melting behaviors, dynamic rheological and foaming properties of PLA would be investigated systematically. The goal of this study was to provide guidance for researching the transition of microcellular to nanocellular structure in PLA foams.

Experimental

Materials

Linear PLA (Grade 2003D) in pellet form with a melt flow rate of 3.2 g/10 min (190 °C, 2.16 kg) was bought from Nature Works Inc. It is a semi-crystalline polymer containing the D-isomer content of approximately 4.3%, the density of 1.24 g/cm^3, the glass transition and melting temperature of 61.4 °C and 147.6 °C, respectively. HG having the diameter of 0.5–3 μm, the thickness of 0.55–3.74 nm, the number of layers less than 10, and the content of oxygen more than 10 wt%, was purchased from J&K Scientific Ltd. Multi-functional epoxy-based chain extender (ADR-4370S) was provided by BASF, Germany and its chemical structure is shown in Fig. 2a.

Preparation of various PLA samples

Prior to melt blending, PLA was dried in a vacuum at 80 °C for 8 h to remove water and mixed with other component in a Haake internal mixer, according to the formula displayed in Table 1. The melting temperature, mixing time, and mixing speed were 190 °C, 15 min, and 60 rpm, respectively. The corresponding sample names were denoted as pure PLA, CPLA, PLA/HG, and CPLA/HG, respectively. Subsequently, the resultant PLA samples were pressed into a sheet by compression molding method at 190 °C and 10 MPa for 10 min and then cooled to room temperature to obtain the sheet samples with the thickness of 1 mm. At least, three samples in each category of various PLA samples were fabricated, according to the preparation method aforementioned and then the small sheet with 1 cm × 1 cm (length × width) was cut in the center of each sample for further characterization and foaming process.

Table 1 Formula of various PLA samples

Sample name	PLA (wt%)	CE (wt%)	HG (wt%)
Pure PLA	100	0	0
CPLA	99	1	0
PLA/HG	99.99	0	0.01
CPLA/HG	98.99	1	0.01

Foaming process of various PLA samples

Various PLA foams were fabricated by the batch foaming method in a stainless steel autoclave using supercritical CO_2 as physical blowing agent. Figure 1 represents the schematic diagram of the autoclave for batch foaming. First, various PLA samples were put into the autoclave for 120 min at a saturation pressure of 10 MPa and the constant foaming temperature of 130, 135 and 140 °C, respectively. After the CO_2 was fully diffused and dissolved in the PLA matrix, the pressure of the autoclave dropped by the release of CO_2 from 10 to 0.1 MPa in about 6 s, which provided a driving force for cell nucleation and growth to obtain various PLA foams.

Characterizations

Differential scanning calorimetry (DSC)

DSC (Q20, TA, USA) was used to study the crystallization and melting behaviors of various PLA sheet samples. PLA sheet samples were equilibrated to 190 °C rapidly under a nitrogen atmosphere, held in the molten state for 5 min to remove prior thermal and stress histories. Subsequently, the samples were cooled to 40 °C and re-heated to 190 °C at a cooling/heating rate of 10 °C/min to record the crystallization and melting behaviors. The relative crystallinity (χ_c) of PLA in various PLA sheet samples was calculated by Eq. (1) [19]:

$$\chi_{C(PLA)} = \frac{\Delta H_{m(PLA)} - \Delta H_{cc(PLA)}}{\Delta H^0_{m(PLA)} \times w_{(PLA)}} \times 100\% \qquad (1)$$

where $\Delta H_{m(PLA)}$ is the melting enthalpy of PLA, $\Delta H_{cc(PLA)}$ is the cold crystallization enthalpy of PLA, $\Delta H^0_{m(PLA)}$ is the melting enthalpy of 100% crystalline PLA that is 93 J/g [20], and W is the weight fraction of PLA in various PLA samples.

Polarized optical microscope (POM)

Spherocrystal morphology of various PLA samples was observed by a POM (BX-51, Olympus, Japan). PLA samples were heated from room temperature to 200 °C at a rate of 30 °C/min, kept for 5 min to eliminate thermal history, and then cooled down at a rate of 10 °C/min to 120 °C and maintained for 40 min to observe the changes of crystal morphology.

Figure 1 Schematic diagram of the autoclave for batch foaming.
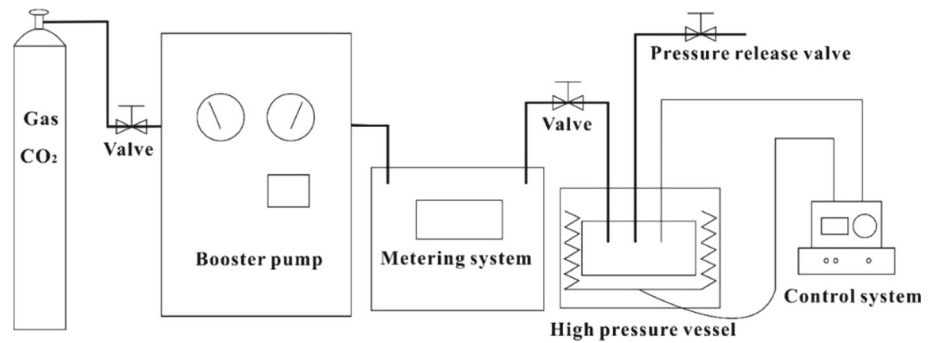
Transmission electron microscope (TEM)

PLA/HG and CPLA/HG were cut into the ultrathin specimens with the thickness of 70 nm for TEM, using a Leica ultramicrotome UC6/UC7 (2017) with a diamond knife. The dispersion of HG in PLA/HG and CPLA/HG was observed using TEM (Tecnai Spirit) under an accelerated voltage of 80 kV.

Scanning electron microscope (SEM)

The fracture surface morphology of various PLA foams was observed by an SEM (FEI, Quanta FEG) at an acceleration voltage of 5 kV. PLA samples were immersed into liquid nitrogen for 4 h, and then fractured. Before observations, the fracture surfaces of various PLA foams were sputter coated with Au to prevent the build-up of electrostatic charge during observations.

Rheological properties

The dynamic rheological properties of various PLA samples were recorded using a rotational rheometer (ARES Rheometer, TA, USA) with a parallel plate (20 mm in diameter with a gap of 1.0 mm) at 190 °C. The angular frequency (ω) range was adjusted from 0.1 to 100 rad/s, and the maximum strain was fixed at 5%, in order to confirm that these conditions were within the linear viscoelastic region under nitrogen. The complex viscosity (η^*), storage modulus (G'), and loss factor (tan δ) of various PLA samples were measured at various ω. Moreover, the η^* of various PLA samples as a function of angular frequency (ω) were also measured in the oscillatory mode at 130, 135, and 140 °C.

Foaming properties

The VER (Φ) of various PLA foams was calculated by Eq. (2):

$$\Phi = \frac{\rho_f}{\rho_p} \tag{2}$$

where ρ_f and ρ_p are the bulk densities of the pre-foam and post-foam samples in g/cm^3, respectively, which were measured by a density balance (Sartorius, Goettingen, Germany).

By assuming the cells were spherical, cell density (N_0) (cells/cm^3) was analyzed by using software image tool and calculated by Eq. (3) [21]:

$$N_0 = \left(\frac{nM^2}{A}\right)^{\frac{3}{2}} \Phi \tag{3}$$

where n is the number of cells in the SEM micrograph, M is the magnification factor, A is the area of the micrograph (cm^2), and Φ is the VER of the PLA foams [22].

Results and discussion

Interactions mechanism between PLA, CE, and/or HG

Two chemical interactions between PLA, CE, and/or HG may occur during the melt mixing process of PLA samples, due to the reactions between the epoxy groups on CE and the hydroxyl and/or carboxyl groups on PLA and HG. The corresponding interaction schematic diagram is represented in Fig. 2b, c. One was the chain extension between PLA and CE, which is shown in Fig. 2b. Another was chemical reaction between PLA, CE and HG, which is displayed in Fig. 2c.

Figure 2 Chemical structure of CE **a** and schematic representation of possible reaction mechanisms between PLA, CE, and HG or not (**b**, **c**).
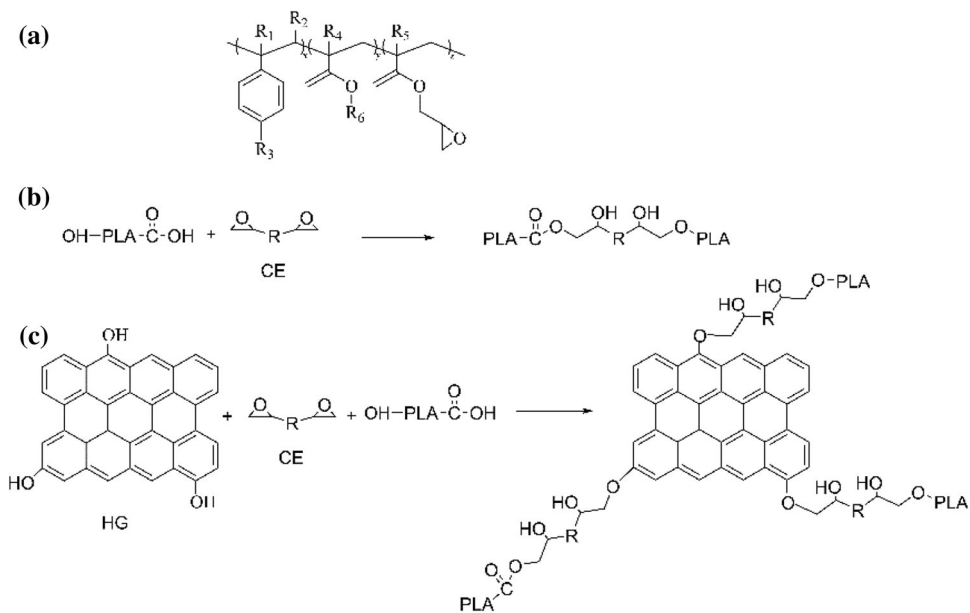
Crystallization and melting behaviors

After the chain extension of PLA, the molecular chain architecture of PLA would transform from linear structure to branching structure [23]. Both the changes in the architecture and the addition of HG would affect the crystallization and melting behaviors of PLA, which would further have a significant impact on the foaming behaviors [24].

Figure 3 shows the DSC curves of various PLA samples at the cooling (a) and heating (b) rates of 10 °C/min. It could be observed in Fig. 3a that there was no apparent crystallization peak in the cooling curve of various PLA samples. This was because the poor flexibility of the molecular chains of PLA restricted the motion of chain segment of PLA and there was not enough time for the crystallization of

PLA molecular chains to be completed during the cooling process [25].

The corresponding cold crystallization temperatures (T_{cc}), T_m, ΔH_m, ΔH_{cc} and χ_c are summarized in Table 2. Both the chain extension and the addition of HG would make the T_{cc} of PLA increase, which may be because the added HG and the resultant branching structures hindered the movement of chain segments of PLA for the crystal growth in the heating process [26, 27]. An interesting phenomenon could be observed in Fig. 3b and Table 2 that the T_{cc} of PLA/HG was slightly higher than that of pure PLA, but the T_{cc} of CPLA/HG was largely higher than that of CPLA, implying that there was a strong interaction between CPLA and HG, maybe the reaction between the hydroxyl groups on HG and the residual epoxy groups on CPLA [35]. In addition, the chain extension

Figure 3 DSC curves of various PLA samples at cooling (**a**) and heating (**b**) rate of 10 °C/min.
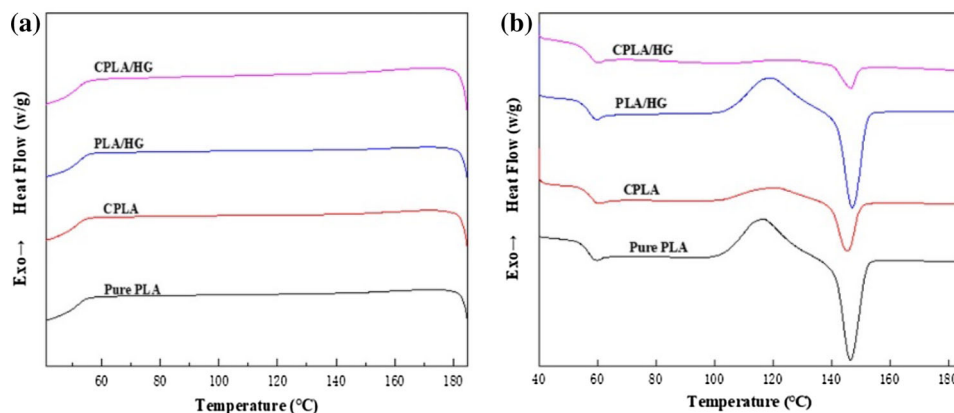
Table 2 Thermal properties of various PLA samples

Sample name	T_{cc} (°C)	T_m (°C)	ΔH_{cc} (J/g)	ΔH_m (J/g)	χ_c (%)
Pure PLA	117.1 ± 0.1	146.5 ± 0.0	23.4 ± 0.1	24.4 ± 0.2	1.0 ± 0.1
CPLA	120.5 ± 0.1	146.7 ± 0.2	9.8 ± 0.2	11.2 ± 0.0	1.5 ± 0.2
PLA/HG	117.9 ± 0.0	147.2 ± 0.1	19.4 ± 0.1	20.6 ± 0.0	1.3 ± 0.0
CPLA/HG	126.1 ± 0.2	146.7 ± 0.0	2.3 ± 0.3	4.3 ± 0.1	2.1 ± 0.2

and the addition of HG had little influence on the T_m of PLA.

From the statistics in Table 2, after the chain extension and/or the addition of HG, the χ_c of PLA was slightly increased. This should be attributed to two aspects. One was that the branching points formed in CPLA could be acted as the homogeneous crystallization nucleation sites [28, 29]. The other was that HG could play a role in heterogeneous crystallization nucleation point during the crystallization process. The two aspects would promote the crystallization process of PLA and further affect its foaming behaviors [30].

POM observation

In order to further study the effect of CE and HG on the crystal morphology of PLA, the number and size of spherocrystals in various PLA samples were observed by POM, as displayed in Fig. 4. A small amount of large spherocrystals could be seen in the POM image of pure PLA, as shown in Fig. 4a. The interfaces between crystalline region and amorphous region were clear, hinting that this was a typical homogeneous nucleation phenomenon [31]. It could be found in Fig. 4b that the number of spherulites in CPLA increased significantly, and the size of spherulites decreased largely. This was because after the addition of the CE, the branching structures were formed in CPLA, which could serve as the sites of crystallization nucleation and promote the number of spherulites [32]. However, the generation of branching structures in CPLA would impede the movement of chain segments into the crystal lattice of CPLA, which restricted the growth of spherocrystals. In other words, the generation of branching structures was beneficial to the crystallization nucleation but

Figure 4 POM images of various PLA samples isothermally crystallized for 40 min at 120 °C: **a** pure PLA, **b** CPLA, **c** PLA/HG, **d** CPLA/HG.
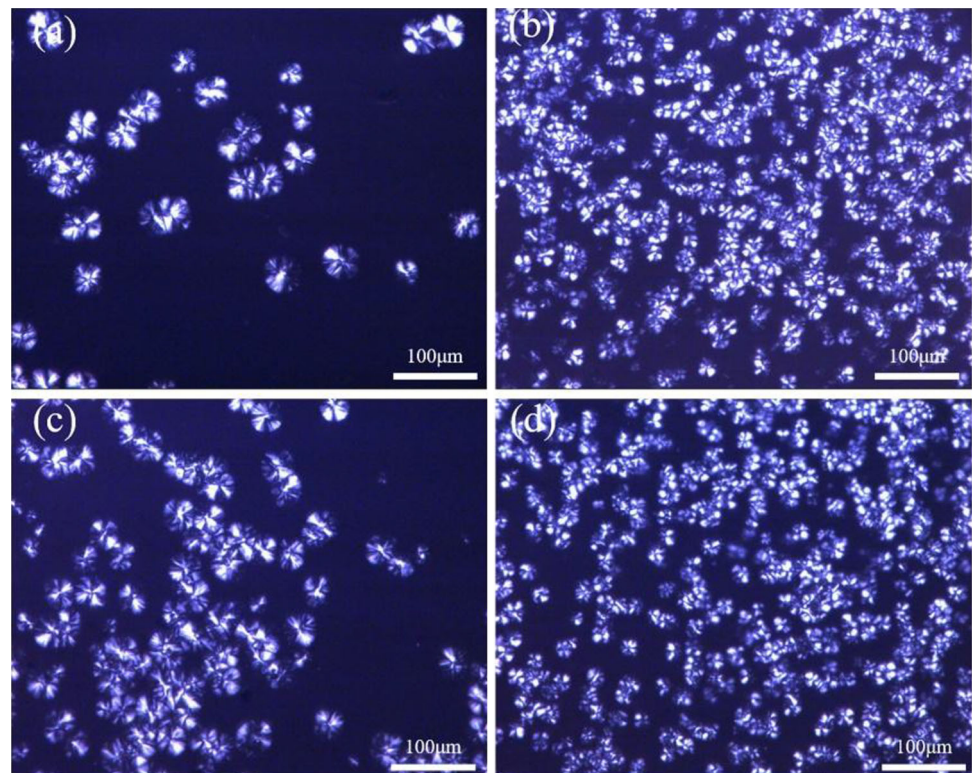
harmful to the crystallization growth, leading to the formation of a large amount of small spherocrystals.

Compared with pure PLA, the number of spherocrystals in PLA/HG increased and their spherocrystal size decreased, as shown in Fig. 4c. This was mainly because the heterogeneous nucleation effect of HG in the crystallization process of PLA improved the crystallization performance of PLA and increased the area of the crystalline region, which was consistent with the trend of χ_c in DSC results. After the introduction of both CE and HG into PLA, many but small spherocrystals could be observed in the POM image of CPLA/HG (Fig. 4d), due to the combined action of CE and HG on the crystallization nucleation and growth of PLA.

Rheological properties

The viscoelasticity of polymer melt was usually tested by the dynamic rotational rheometer. The shear rheological parameters (η^*, G' and tan δ) of polymer melt are very sensitive to the changes in the molecular chain structure of polymer as well as the content and type of added fillers [33].

The η^* has an important influence on the cell growth. If the η^* is too low, the phenomenon of cell mergence and cell rupture would be aggravated and the blowing agent in the foaming system would escape, leading to high density and low VER. If the η^* is too high, the cell growth would be hindered greatly, resulting in the decrease in cell size [34]. Figure 5a shows the relationship between η^* of various PLA samples and ω. In Fig. 5a, all the four PLA samples (pure PLA, PLA/HG, CPLA and CPLA/HG) exhibited typical shear-thinning phenomenon of pseudoplastic fluid in the range of ω from 0.1 to 100 rad/s. The η^* of CPLA and CPLA/HG was much higher than that of pure PLA and PLA/HG, indicating that the addition of the CE had a significant effect on increasing the η^* of PLA, especially at low ω. This was mainly because the formation of branching structures increased the relaxation time and viscosity of PLA [35].

The relationship between G' of various PLA samples and ω is represented in Fig. 5b. The G' could reflect the melt elasticity of polymer, which was one of the important indexes to measure the melt strength and foamability of polymer. The bigger the G', the better the melt elasticity and melt strength were, the higher the foamability was [36]. In Fig. 5b, the G' of

CPLA and CPLA/HG was higher than that of pure PLA and PLA/HG, especially in the low ω regions, suggesting that a longer relaxation mechanism existed [37]. The branching molecular chains in CPLA and CPLA/HG could be easily entangled with their surrounding other PLA molecular chains. These entanglement points could be acted as temporary cross-linking sites to improve the elasticity of PLA melt [38]. Similar shear rheological behaviors were found in other branching PLA system [39]. Besides that, it could be also found in Fig. 5a, b that compared with pure PLA and CPLA, both η^* and G' of PLA/HG and CPLA/HG increased. This maybe because the introduction of HG hindered the motion of PLA and CPLA molecular chains as well as the hydroxyl groups on the HG reacted with the remaining epoxy groups on CPLA in CPLA/HG system.

In Fig. 5c, it could be seen that the big peak of mechanical loss appeared at the ω around 1 rad/s in the tan δ curves of pure PLA and PLA/HG, respectively. The tan δ of CPLA and CPLA/HG decreased gradually as the ω increased, indicating their mechanical loss peaks at the low ω, at least below 0.1 rad/s. The lower the ω at the mechanical loss peak, the longer the relaxation time was. After the addition of CE, the tan δ of CPLA and CPLA/HG was much lower than that of pure PLA and PLA/HG, suggesting that the elastic response became fast, the viscous dissipation decreased gradually and thus the foamability was enhanced [39]. This could be attributed to the fact that the formation of branching structures enhanced the number of entanglements between PLA molecular chains. These entanglements could be acted as physical network points to enhance the melt elasticity of CPLA and CPLA/HG [37].

The dispersion of HG in PLA matrix

For polymeric composites, the dispersion of fillers is vital to the properties of final product [40]. The dispersion status of HG in PLA/HG and CPLA/HG was observed by TEM. Figure 6a, b represents the TEM images of PLA/HG and CPLA/HG, respectively. In Fig. 6a, some HG aggregation of could be seen, indicating the poor dispersion of HG in PLA matrix. As comparison, after HG was added into PLA matrix during the chain extension, the size of HG aggregation decreased and the number of small HG aggregation increased, indicating that the aggregation of

Figure 5 Dynamic shear rheological properties of various PLA samples versus ω at the temperature of 190 °C: **a** η^*, **b** G', **c** tan δ.
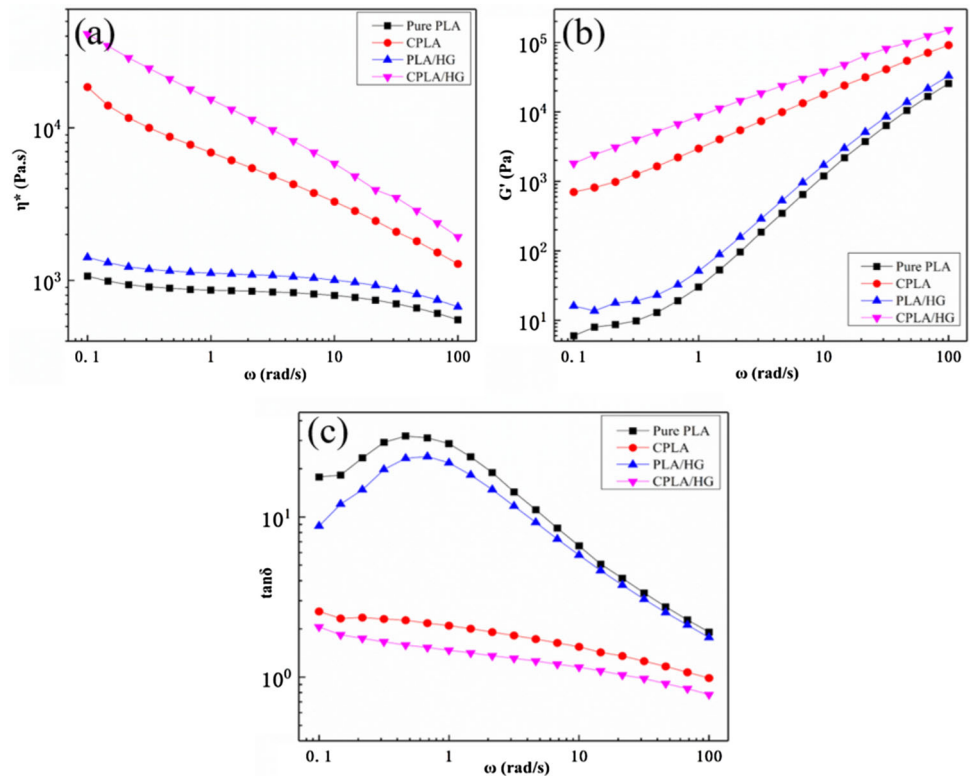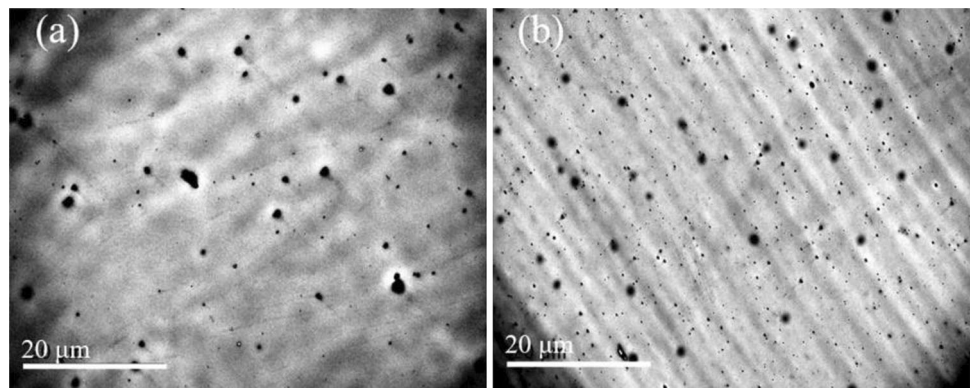

Figure 6 TEM images of PLA/HG (**a**) and CPLA/HG (**b**).

HG in PLA matrix released (Fig. 6b). The reason may be that the hydroxyl group on HG reacted with the epoxy group on CE during the chain extension, and HG was indirectly connected with the molecular chains of CPLA, which was helpful for the good dispersion of HG in CPLA matrix.

Foaming properties

Because the transition temperature from microcellular to nanocellular structure in pure PLA foams and PLA/HG foams had a large different from that in CPLA foams and CPLA/HG foams, all the four PLA foams (pure PLA foam, PLA/HG foam, CPLA foam and CPLA/HG foam) were divided into two categories for discussion. One was the pure PLA foams and PLA/HG foams at the foaming temperature of 140 °C and 135 °C, respectively. The other was CPLA foams and CPLA/HG foams at the foaming temperature of 135 °C and 130 °C, respectively.

Figures 7 and 8 show the cellular morphology and cell number frequency distribution of pure PLA foams and PLA/HG foams at the foaming temperature of 140 °C and 135 °C, respectively. The corresponding cellular parameters of pure PLA foams and PLA/HG foams are summarized in Table 3.

Figure 7 SEM images of the cellular morphology of various PLA foams: **a** pure PLA foam, 140 °C; **b** PLA/HG foam, 140 °C; **c** pure PLA foam, 135 °C; **d** PLA/HG foam, 135 °C.
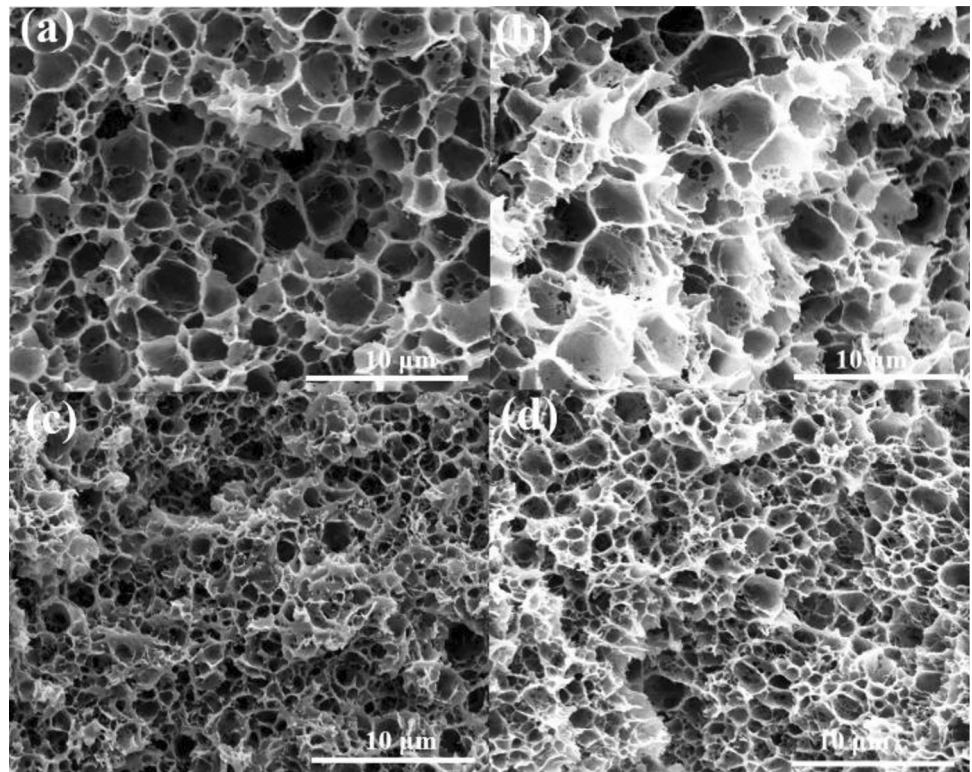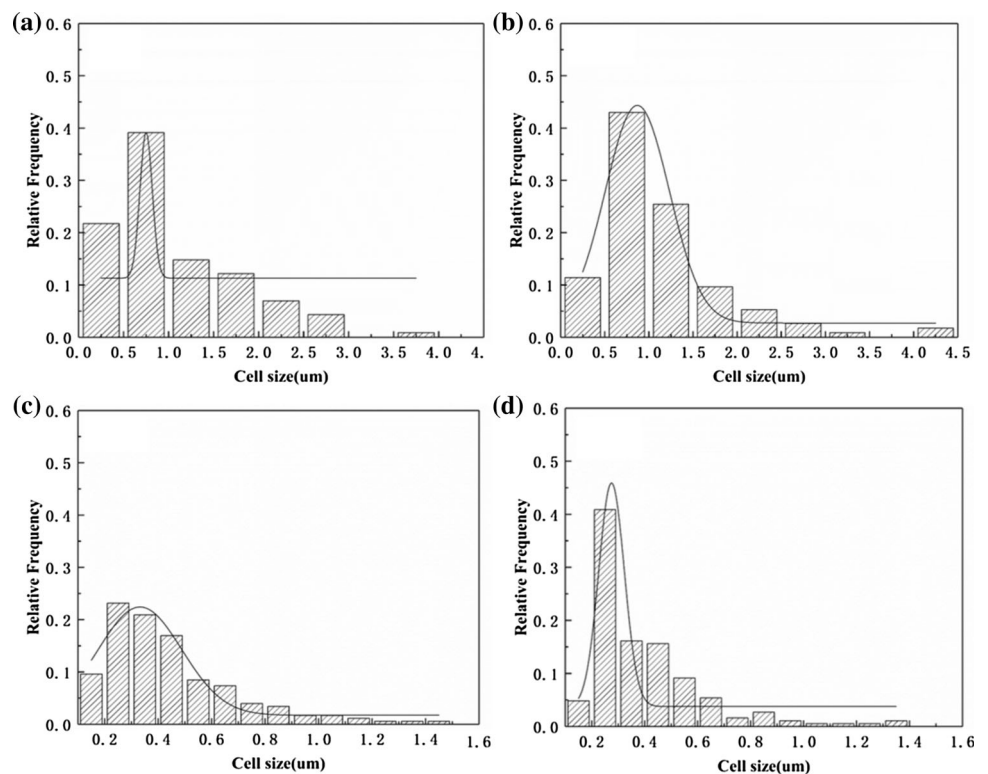

Figure 8 Cell number frequency distribution of various PLA foams: **a** pure PLA foam, 140 °C; **b** PLA/ HG foam, 140 °C; **c** pure PLA foam, 135 °C; **d** PLA/HG foam, 135 °C.

It could be found in Fig. 7 and Table 3 that microcells appeared in pure PLA foam and PLA/HG foams at 140 °C. When the foaming temperature decreased from 140 to 135 °C, an obvious transition from microcells to nanocells in pure PLA foams and PLA/HG foams was observed. For pure PLA foams,

Table 3 The cellular parameters of pure PLA foams and PLA/HG foams at 140 °C and 135 °C, respectively

Sample name	Cell size (nm)	Cell density (cells/cm^3)	VER
140 °C			
Pure PLA	$1.07 \times 10^3 \pm 0.51 \times 10^3$	1.19×10^{12}	3.65 ± 0.23
PLA/HG	$1.04 \times 10^3 \pm 0.70 \times 10^3$	1.89×10^{12}	6.30 ± 0.17
135 °C			
Pure PLA	440 ± 247	5.77×10^{12}	1.51 ± 0.31
PLA/HG	400 ± 222	5.95×10^{12}	1.73 ± 0.14

the average cell size was 440 ± 247 nm, the density was about 5.77×10^{12} cells/cm^3, and the VER was 1.51 ± 0.31 times. When HG was added into PLA, the average cell size of PLA/HG foams decreased to 400 ± 222 nm, their cell density and VER increased to 5.95×10^{12} cells/cm^3 and 1.73 ± 0.14 times, slightly and respectively. This should be attributed to the heterogeneous nucleating effect of HG for the cell nucleation and the crystallization nucleation as well as the improvement of the rheological properties of PLA by the addition of HG [41–43].

Compared with those of pure PLA foam and PLA/HG foam prepared at 140 °C, the cell size and VER of pure PLA foam and PLA/HG foam decreased and their cell density increased, respectively, at the foaming temperature of 135 °C. This was because with the foaming temperature decreasing, the viscosity of PLA increased, which was helpful for restricting cell growth and mergence as well as result in small cell, high cell density and low VER [44]. Foaming temperature had a significant effect on tailoring the cellular structure and foaming properties of semi-crystalline polymer, especially for the generation of nanocellular foams [45].

The cell number frequency distribution of pure PLA foams and PLA/HG foams at 140 and 135 °C is shown in Fig. 8. It could be found that the addition of HG had little effect on the cell size distribution of pure PLA foam and PLA/HG foam. However, foaming temperature had a great influence on the cell size distribution of pure PLA foam and PLA/HG foam, which was mainly related to the changes of viscoelasticity.

Figures 9 and 10 illustrate the SEM micrographs and cell number frequency distribution of CPLA foams and CPLA/HG foams at the foaming temperature of 135 °C and 130 °C, respectively. The corresponding cellular parameters of CPLA foams and CPLA/HG foams are displayed in Table 4.

It could be seen from Fig. 9 and Table 4, with the foaming temperature of 135 °C, the cell size of CPLA foam and CPLA/HG foam were in microcellular rank. When the foaming temperature decreased from 135 to 130 °C, a similar transition from microcells to nanocells occurred in CPLA foams and CPLA/HG foams. Especially, the cell size of CPLA/HG foams could reach 350 ± 247 nm. At the same time, the cell density of CPLA foams and CPLA/HG foams increased largely and their VER decreased for several times. The VER of various PLA foams exhibited great sensitivity as a function of temperature, obviously due to their viscosity, and therefore matrix stiffness was more sensitive to temperature (Fig. 11). Similar phenomenon was found in other study [15]. After the introduction of HG into PLA matrix, it could be observed in Table 4 that the change trend on the cell size, cell density and VER in CPLA foam and CPLA/HG foam were similar to those of pure PLA foam and PLA/HG foam, because HG could be served as the heterogeneous cell nucleation point.

It could be found in Fig. 10 that the addition of HG in CPLA/HG foams had a little influence on the cell size distribution but decreasing foaming temperature had a great effect on the cell size distribution.

In order to investigate the effect of chain extension on the cellular parameters and cell size distribution, the four PLA foams prepared at 135 °C were chosen and employed to study. As shown in Tables 3 and 4, when the foaming temperature was 135 °C, CPLA foam and CPLA/HG foam had larger cell size, lower cell density and higher VER than pure PLA foam and PLA/HG foam. The main reason was that the melt strength of PLA was improved by the formation of branching structure. In the process of cell growth, the foaming agent escaped slowly and the cells had sufficient time to grow or merge, leading to large cell size and high VER. After the addition of CE, the cell size distribution of PLA became broad significantly. Similar phenomenon was observed in our previous study [46].

Figure 9 SEM images of the cellular morphology of various PLA foams: **a** CPLA foam, 135 °C; **b** CPLA/HG foam, 135 °C; **c** CPLA foam, 130 °C; **d** CPLA/HG foam, 130 °C.
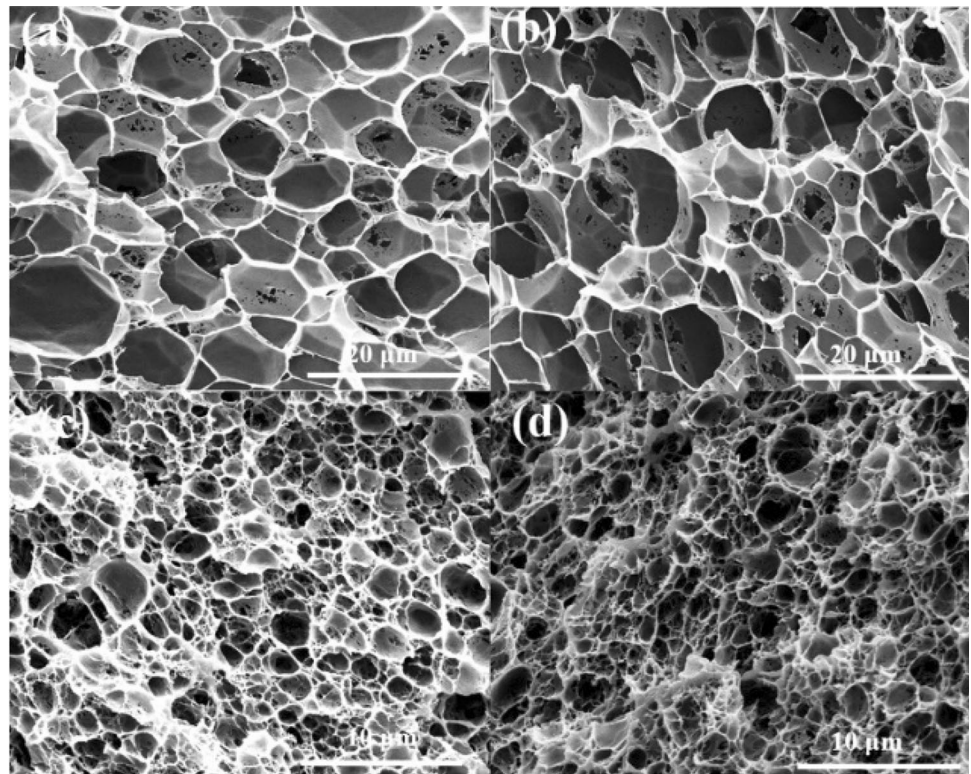

Figure 10 Cell number frequency distribution of various PLA foams: **a** CPLA foam, 135 °C; **b** CPLA/HG foam, 135 °C; **c** CPLA foam, 130 °C; **d** CPLA/HG foam, 130 °C.
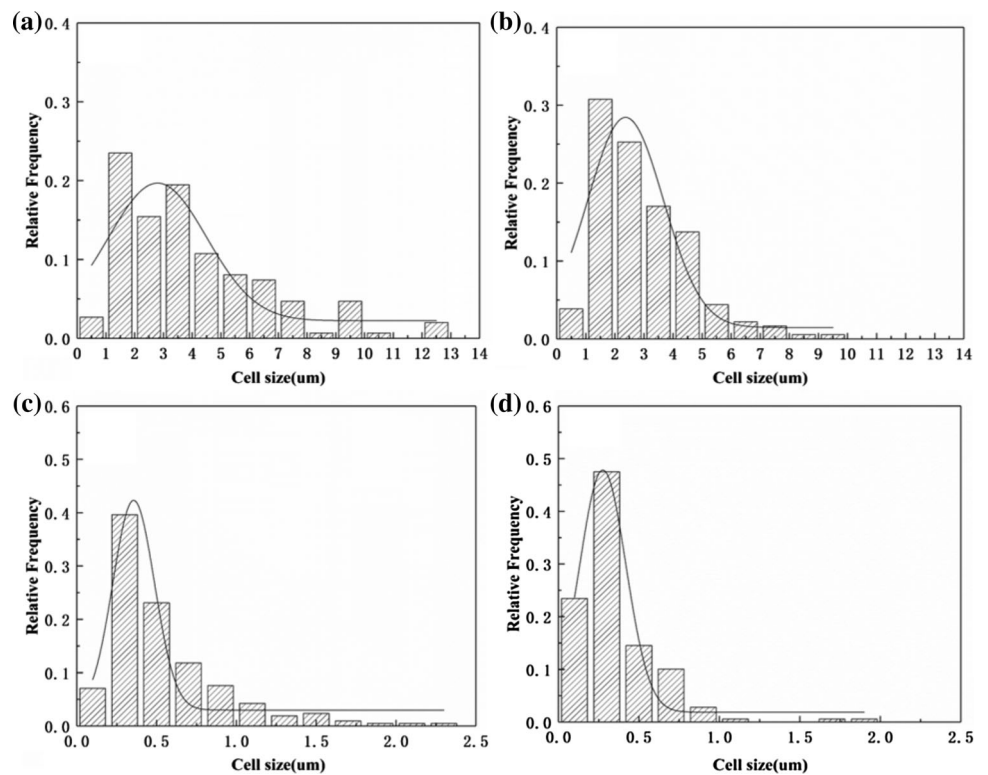
Table 4 The cellular parameters of CPLA foams and CPLA/HG foams at 135 °C and 130 °C, respectively

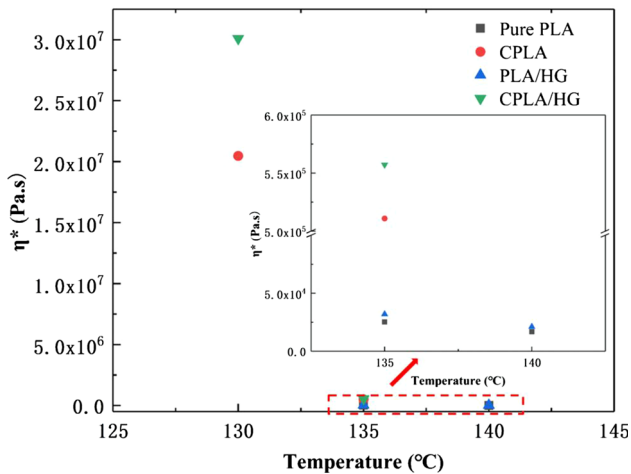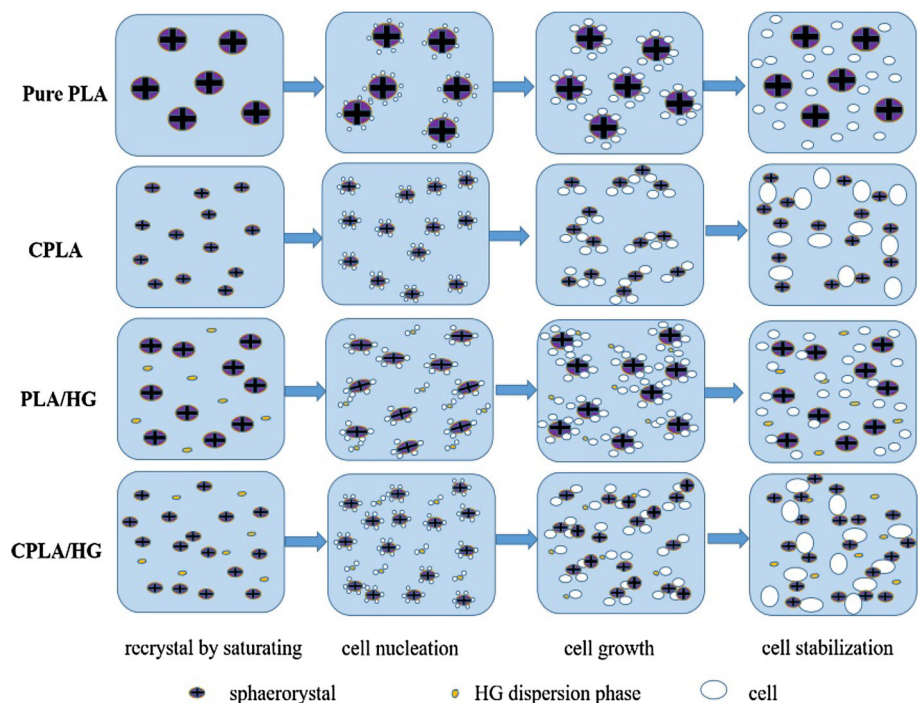| Sample name	Cell size (nm)	Cell density (cells/cm³)	VER
135 °C			
CPLA	$4.03 \times 10^3 \pm 2.59 \times 10^3$	2.74×10^{11}	25.00 ± 0.39
CPLA/HG	$2.91 \times 10^3 \pm 1.60 \times 10^3$	3.73×10^{11}	25.20 ± 0.35
130 °C			
CPLA	530 ± 380	1.81×10^{12}	2.72 ± 0.10
CPLA/HG	350 ± 247	1.76×10^{13}	3.71 ± 0.16

Figure 11 η^* of various PLA samples at 0.1 rad/s as a function of foaming temperature (130, 135 and 140 °C). The inset shows the η^* measured at 135 and 140 °C.

Foaming mechanism

According to the classical cell nucleation theory, the cell nucleation of polymer foams could be divided into homogeneous nucleation and heterogeneous nucleation [47]. Homogeneous cell nucleation would happen when sufficient dissolved blowing agent gas formed clusters for a long enough time to make a critical cell radius. Heterogeneous cell nucleation was the most common type of cell nucleation for polymer foam, which was generally generated at the interface between the additive or second polymer phase and the matrix phase. The presence of the interface could reduce the activation energy for acquiring a stable cell and increase the number of cell nucleation points.

Figure 12 demonstrates the schematic diagram for the cell formation of the four PLA foams. For the cell nucleation process, since the foaming temperature was constant and slightly lower than T_{m}, numerous

Figure 12 The cell formation schematics of the four PLA foams.

relative perfect spherocrystals in PLA matrix would not be melt, acting as the cell nucleation points. Some cells would be generated at the interfaces between the crystalline region and amorphous region in the four PLA foams. On the other hand, some HG reserved possibly in the amorphous region of PLA/HG or CPLA/HG, and some cells may occur at the interfaces between PLA matrix and HG. For the cell growth and stabilization process, the immediately cooling after depressurization and the presence of numerous crystalline regions would limit the cell growth, resulting in nanocellular or microcellular PLA foams.

Conclusion

In this paper, CE and HG were introduced into PLA through melt blending method to improve the crystallization behaviors, rheological properties and supercritical CO_2 foaming performance of PLA. An interesting phenomenon was observed in DSC results that the T_{cc} of PLA/HG was slightly higher than that of pure PLA, but the T_{cc} of CPLA/HG was greatly higher than that of CPLA, due to the strong interaction between CPLA and HG. Compared with other PLA samples, many but small spherocrystals were observed in the POM image of CPLA/HG. The TEM observation displayed that after HG was added into PLA matrix during the chain extension, HG aggregation became numerous and small.

Nanocellular PLA foams were fabricated successfully using a facile batch foaming method with constant foaming temperature slightly lower than T_m. The transition temperature from microcells to nanocells in various PLA foams was confirmed. The foaming parameters of CPLA/HG foam fabricated at 130 °C were optimum, its cell size could reach 350 ± 247 nm as well as its cell density and VER were 1.76×10^{13} cells/cm^3 and 3.71 ± 0.16 times, respectively. Compared with the addition of HG, foaming temperature and chain extension had a significant influence on the cell size distribution of PLA foams.

Funding

Compliance with ethical standards

Conflict of interest The authors declare that they have no competing interests.

References

[1] Okolieocha C, Raps D, Subramaniam K, Altstadt V (2015) Microcellular to nanocellular polymer foams: progress (2004–2015) and future directions—a review. Eur Polym J 73:500–519

[2] Muanchan P, Ito H (2018) Nanocellular foams confined within PS microfibers obtained by CO_2 batch foaming process. Microsyst Technol 24:655–662

[3] Nofar M, Park CB (2014) Poly(lactic acid) foaming. Prog Polym Sci 39:1721–1741

[4] Yeh SK, Chen YR, Kang TW et al (2018) Different approaches for creating nanocellular TPU foams by supercritical CO_2 foaming. J Polym Res 25:30

[5] Leon MD, Bernardo V, Rodriguez-Perez MA (2017) Key production parameters to obtain transparent nanocellular PMMA. Macromol Mater Eng 302:1700343

[6] Luo Y, Ye C (2012) Using nanocapsules as building blocks to fabricate organic polymer nanofoam with ultra low thermal conductivity and high mechanical strength. Polymer 53:5699–5705

[7] Forest C, Chaumont P, Cassagnau P, Swoboda B, Sonntag P (2015) Polymer nano-foams for insulating applications prepared from CO_2 foaming. Prog Polym Sci 41:122–145

[8] Ling J, Zhai W, Feng W, Shen B, Zhang J, Zheng WG (2013) A facile preparation of lightweight microcellular polyetherimide/graphene composites foams for electromagnetic interference (EMI) shielding. Acs Appl Mater Interfaces 5:2677–2684

[9] Gaspard S, Oujja M, Nalda RD, Castillejo M, Banares L, Lazare S, Bonneau R (2008) Nanofoaming dynamics in biopolymers by femtosecond laser irradiation. Appl Phys A 93:209–213

[10] Reignier J, Huneault MA (2006) Preparation of interconnected poly(3-caprolactone) porous scaffolds by a combination of polymer and salt particulate leaching. Polymer 47:4703–4717

[11] Hong SM, Hwang SS (2006) A nanofoaming process and dielectric properties of polymethylphenylsilsesquioxane-based nanofoams. J Appl Polym Sci 100:4964–4971

[12] Costeux S (2014) CO$_2$-blown nanocellular foams. J Appl Polym Sci 41293:1–16

[13] Costeux S, Zhu L (2013) Low density thermoplastic nanofoams nucleated by nanoparticles. Polymer 54:2785–2795

[14] Guo H, Kumar V (2015) Some thermodynamic and kinetic low-temperature properties of the PC-CO$_2$ system and morphological characteristics of solid-state PC nanofoams produced with liquid CO$_2$. Polymer 56:46–56

[15] Tiwary P, Park CB, Kontopoulou M (2017) Transition from microcellular to nanocellular PLA foams by controlling viscosity, branching and crystallization. Eur Polym J 91:283–296

[16] Yi XJO, Lai YL, Davoodi P, Wang CH (2018) Production of drug-releasing biodegradable microporous scaffold using a two-step micro-encapsulation/supercritical foaming process. J Supercrit Fluid 133:263–269

[17] Lee ST (2004) Thermoplastic foam processing: Principles and development. CRC Press, Boca Raton

[18] Zhao H, Cui Z, Wang X, Turng LS, Peng X (2013) Processing and characterization of solid and microcellular poly(lactic acid)/polyhydroxybutyrate-valerate (PLA/PHBV) blends and PLA/PHBV/Clay nanocomposites. Compos Part B Eng 51:79–91

[19] Wang X, Liu W, Zhou H, Liu B, Li H, Du Z, Zhang C (2013) Study on the effect of dispersion phase morphology on porous structure of poly(lactic acid)/poly(ethylene terephthalate glycol-modified) blending foams. Polymer 54:5839–5851

[20] Lu X, Tang L, Wang L, Zhao J, Li D, Wu Z, Xiao P (2016) Morphology and properties of bio-based poly(lactic acid)/high-density polyethylene blends and their glass fiber reinforced composites. Polym Test 54:90–97

[21] Wang Z, Ding X, Zhao M, Wang X, Xu G, Xiang A, Zhou H (2017) A cooling and two-step depressurization foaming approach for the preparation of modified HDPE foam with complex cellular structure. J Supercrit Fluid 125:22–30

[22] Mihai M, Huneault MA, Favis BD, Li H (2007) Extrusion foaming of semi-crystalline PLA and PLA/thermoplastic starch blends. Macromol Biosci 7:907–920

[23] Chen P, Zhou H, Liu W, Zhang M, Du Z, Wang X (2015) The synergistic effect of zinc oxide and phenylphosphonic acid zinc salt on the crystallization behavior of poly(lactic acid). Polym Degrad Stab 122:25–35

[24] Liu W, Chen P, Wang X, Wang F, Wu Y (2017) Effects of poly(butyleneadipate-co-terephthalate) as a macromolecular nucleating agent on the crystallization and foaming behavior of biodegradable poly(lactic acid). Cell Polym 36:75–96

[25] Nerkar M, Ramsay JA, Ramsay BA, Kontopoulou M (2015) Dramatic improvements in strain hardening and crystallization kinetics of PLA by simple reactive modification in the melt state. Macromol Mater Eng 299:1419–1424

[26] Bouakaz BS, Habi A, Grohens Y, Pillin I (2017) Organomontmorillonite/graphene-PLA/PCL nanofilled blends: new strategy to enhance the functional properties of PLA/PCL blend. Appl Clay Sci 139:81–91

[27] Zhao JC, Du FP, Zhou XP et al (2011) Thermal conductive and electrical properties of polyurethane/hyperbranched poly(urea-urethane)-grafted multi-walled carbon nanotube composites. Compos Part B Eng 42:2111–2116

[28] Zhou H, Wang X, Du Z, Li H, Yu K (2015) Preparation and characterization of chain extended poly(butylene succinate) foams. Polym Eng Sci 55:988–994

[29] Wang X, Zhang Y, Liu B, Du Z, Li H (2008) Crystallization behavior and crystal morphology of linear/long chain branching polypropylene blends. Polym J 40:450–454

[30] Sullivan EM, Yun JO, Gerhardt RA, Wang B, Kalaitzidou K (2014) Understanding the effect of polymer crystallinity on the electrical conductivity of exfoliated graphite nanoplatelet/polylactic acid composite films. J Polym Res 21:563

[31] Qi F, Tang M, Chen X, Chen M, Guo G, Zhang Z (2015) Morphological structure, thermal and mechanical properties of tough poly(lactic acid) upon stereocomplexes. Eur Polym J 71:314–324

[32] Pantani R, Santis FD, Sorrentino A, Maio FD, Titomanlio G (2010) Crystallization kinetics of virgin and processed poly(lactic acid). Polym Degrad Stabil 95:1148–1159

[33] Zhao M, Ding X, Mi J, Zhou H, Wang X (2017) Role of high-density polyethylene in the crystallization behaviors, rheological property, and supercritical CO$_2$ foaming of poly(lactic acid). Polym Degrad Stab 146:277–286

[34] Kuang TR, Mi HY, Fu DJ, Jing X, Chen BY, Mou WJ, Peng XF (2015) Fabrication of poly(lactic acid)/graphene oxide foams with highly oriented and elongated cell structure via unidirectional foaming using supercritical carbon dioxide. Ind Eng Chem Res 54:758–768

[35] Wang X, Zhou H, Liu B, Du Z, Li H (2015) Chain extension and foaming behavior of poly(lactic acid) by functionalized multiwalled carbon nanotubes and chain extender. Adv Polym Technol 33:21444

[36] Chen L, Rende D, Schadler LS, Ozisik R (2013) Polymer nanocomposite foams. J Mater Chem A 1:3837–3850

[37] Mihai M, Huneault MA, Favis BD (2010) Rheology and extrusion foaming of chain-branched poly(lactic acid). Polym Eng Sci 50:629–642

[38] Kolodka E, Wang W, Zhu S, Hamielec AE (2004) Rheological and thermomechanical properties of long-chain-branched polyethylene prepared by slurry polymerization with metallocene catalysts. J Appl Polym Sci 92:307–316

[39] Rajagopalan G, Immordino KM Jr, Gillespie JW, Mcknight SH (2000) Diffusion and reaction of epoxy and amine in polysulfone studied using fourier transform infrared spectroscopy: experimental results. Polymer 41:2591–2602

[40] Liu C, Ye S, Feng J (2017) Promoting the dispersion of graphene and crystallization of poly(lactic acid) with a freezing-dried graphene/PEG masterbatch. Compos Sci Technol 144:215–222

[41] Li K, Cui Z, Sun X, Turng LS, Huang H (2011) Effects of nanoclay on the morphology and physical properties of solid and microcellular injection molded polyactide/poly(butylenes adipate-co-terephthalate) (PLA/PBAT) nanocomposites and blends. J Biobased Mater Bioenergy 5:442–451

[42] Najafi N, Heuzey MC, Carreau PJ, Therriault D, Park CB (2014) Rheological and foaming behavior of linear and branched polylactides. Rheol Acta 53:779–790

[43] Zhang Y, Tiwary P, Parent JS, Kontopoulou M, Park CB (2013) Crystallization and foaming of coagent-modified polypropylene: nucleation effects of cross-linked nanoparticles. Polymer 54:4814–4819

[44] Nofar M, Guo Y, Park CB (2013) Double crystal melting peak generation for expanded polypropylene bead foam manufacturing. Ind Eng Chem Res 52:2297–2303

[45] Nofar M, Zhu W, Park CB (2012) Effect of dissolved CO_2 on the crystallization behavior of linear and branched PLA. Polymer 53:3341–3353

[46] Liu H, Wang X, Zhou H, Liu W, Liu B (2015) The Preparation and characterization of branching poly(ethylene terephthalate) and its foaming behavior. Cell Polym 34:63–94

[47] Colton JS, Suh NP (1987) Nucleation of microcellular foam: theory and practice. Polym Eng Sci 27:500–503